THE EFFECTS OF A MOUNTAIN ON THE PROPAGATION OF PRE-EXISTING CONVECTION FOR DIFFERENT FROUDE NUMBER FLOW REGIMES

Heather Dawn Reeves and Yuh-Lang Lin

Marine, Earth and Atmospheric Sciences North Carolina State Univ., Box 8208 Raleigh, NC 27695-8208
Email: *hdreeves@unity.ncsu.edu*

Abstract: In this research, the tendency for squall lines to stagnate upstream of mountain ranges is investigated through a series of 2-dimensional, idealized simulations where the basic state wind was varied from 1 m s^{-1} to 20 m s^{-1}. These simulations included a set of simulations with no pre-existing convection but with a mountain (MO), a set with pre-existing convection, but no mountain (SO), and a set with both the pre-existing convection and the mountain (SM). These simulations show stagnation is dependent on the Froude number of the basic state flow with stagnation appearing to occur for smaller Froude number flow regimes. For subcritical Froude number flow, the greatest precipitation accumulations were found well upstream of the mountain. This maximum in precipitation was larger than that for either the MO and SO simulations and, additionally, was farther upstream than the maxima in either of these simulations. For critical Froude number flow, the SM simulations exhibited two precipitation maxima. The upstream maximum was colocated with the precipitation maximum in the SO simulation, while the downstream maxima was colated with that in the MO simulation. Finally, for supercritical flow, the precipitation maximum in the SM simulation was positioned over the peak of the mountain. This maximum was smaller than in the MO simulation.

1. INTRODUCTION

The aim of this research is to learn how orography alters the propagation and precipitation for pre-existing convection lines: a topic inspired by some findings from the Mesoscale Alpine Programme (MAP; Bougeault et al. 2001). Accumulated precipitation analyses based on raingauge observations from MAP show three cases of high precipitation accumulation in the Rhône River drainage basin, which is situated just west of the French Alps; IOP-3, IOP-9, and IOP-10. These analyses are shown in Fig. 1.

In each of these cases, a squall line approached the French Alps from the west. As the squall lines impinged on the orography, they stagnated on the upstream side of the mountain. In other cases during MAP where a squall line approached the French Alps from the west, stagnation was not observed. Rather, the convective lines appear to have traversed over the orography with little alteration to their forward translation speed. The accumulated precipitation on the western side of the Alps for these non-stalled cases was significantly less than in the stalled cases. Similar phenomena has been noted during the TAMEX field program. It has been suggested by Teng et al. (2000) that the tendency for some convective lines to stall upstream of the orography is dependent upon the Froude number of the basic state flow. The Froude number for stratified, moist flow is given by

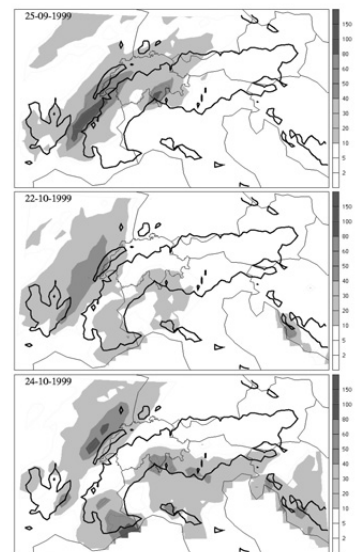$$F_w = \frac{U}{N_w h} \qquad (1)$$

Figure 1: The 24 h accumulated precipitation starting at 06 UTC on the day given in the upper left of each panel.

where U is the basic state wind speed, h is the mountain height, and N_w is the moist Brunt-Vaisala frequency (Chen and Lin 2005). A subcritical, or low F_w, flow regime is defined as having an upstream propagating density current. In the supercritical or high F_w flow regime, both density currents associated with the orographically induced convection are advected downstream by the relatively stronger basic state flow. A critical regime is defined as having a stationary density current over the peak or upslope of the mountain (Chu and Lin 2000).

Herein we test whether or not F_w dictates the tendency for squall line stagnation on the upstream side of orographic barriers.

2. EXPERIMENTAL DESIGN

Experiments were performed using ARPS v5.1.0 (Xue et al. 2001). This model solves the fully compressible, three-dimensional, nonhydrostatic equations in terrain following height $(\sigma - z)$ coordinates. Fourth and second order advection schemes were used in the horizontal and vertical directions, respectively. The horizontal grid spacing was 1 km with 1000 grid points in the north-south direction. The vertical grid spacing was stretched from 50 m at the bottom of the domain to 351 m at the domain top. There are 80 vertical levels which give a domain height of 20 km. The boundary conditions in the east and west (north and south) directions were radiation (periodic). The lower boundary was free slip. A sponge layer was applied above 14 km to reduce artificial wave reflection by the upper boundary. In all simulations, the model time step is 3 seconds. Each simulation was integrated for 12 hours. Microphysical processes were parameterized based on Lin et al. (1983).

The French Alps were represented by an idealized, two-dimensional mountain geography given by

$$h = \frac{h_m a^2}{(x - x_0)^2} \qquad (2)$$

where h_m is the maximum terrain height (2 km), a is the mountain half width (30 km), and x_0 is the location of the mountain center (600 km from the west boundary). Each simulation was initialized using the Weisman-Klemp (1982; Fig. 2) sounding and a constant wind profile that varied from 1 m s^{-1} to 20 m s^{-1}.

There were three sets of experiments, one with a mountain, but no pre-existing convection. In this set of simulations, all convection was induced by the orography. These simulations are referred to as the MO simulations. In the second set of experiments, there was no orography. Line convection was triggered by a surface, soup-can shaped potential temperature perturbation of -18 K situated 400 km from the western boundary. This perturbation had a radius of 5 km and was 2.5 km deep. These simulations are referred to as the SO simulations. The third set of experiments had both a mountain and the temperature perturbation. This final set of experiments, referred to as the SM simulations, represents flow impinging on an orographic barrier with an embedded, pre-existing convective line.

Figure 2: Sounding used to initialize simulations (temperature - black, dew point temperature - red) from Weisman and Klemp 1982).

The MO and SO simulations revealed that for wind speeds less than 10 m s^{-1}, the flow was sub-critical. For $U = 10$ and 11 m s^{-1}, the flow was critical and for U greater than 11 m s^{-1} the flow was supercritical.

3. RESULTS

An overall impression of the combined effects of the squall line and mountain can be gained through inspection of the accumulated precipitation for cases from each regime (Fig. 3). For the supercritical case (Fig. 3a), there is a precipitation maximum over the peak of the mountain for both the SM15 and MO15 cases. The total accumulation was somewhat less in the SM15 case than in the MO15 case, a fact that can be understood through inspection of the perturbation potential temperature fields for the SM15 and MO15 cases (Fig. 4).
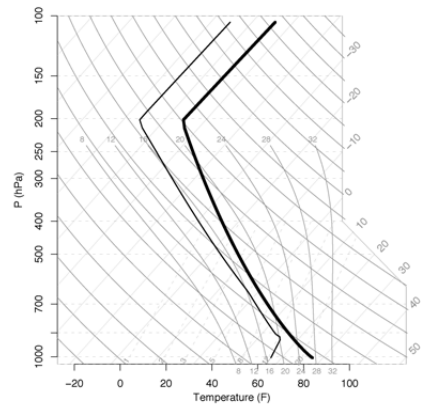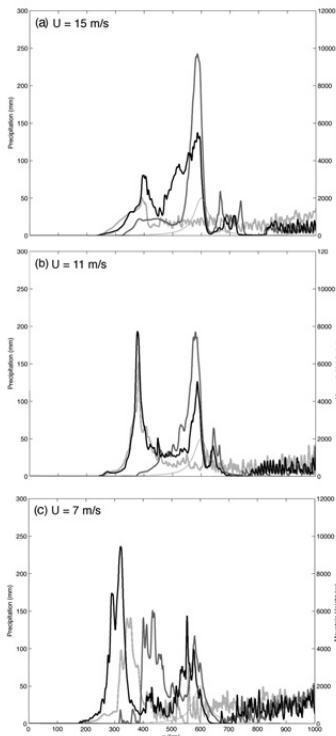
Figure 3: The 12 h accumulated precipitation for $U =$ (a) 7 m s^{-1}, (b) 11 m s^{-1}, and (c) 15 m s^{-1}. The MO cases are given by the red curve, the SO by the blue curve and the SM cases by the green curve.

In the SM15 case, evaporative cooling due to the pre-existing convection acted to cool the lowest layer of the atmosphere immediately upstream of the mountain. This cooling acted to stablilize the lowest part of the air columns impinging on the mountain which acted to reduce the Froude number and shift the flow to a lower Froude number flow regime. Indeed, the u wind field immediately upstream of the mountain (Fig. 4) shows the wind near the surface in the SM15 case was much weaker than that for the MO15 case. In fact, in the lowest 300 m, the flow in the SM15 case was upstream. According to linear theory,

$$ w \propto U \frac{\partial h}{\partial x} \quad . \tag{3} $$

Hence, in the SM15 case, the weaker winds lead to a smaller w which, in turn, appears to have led to reduced precipitation.

In the critical case ($U = 11$ m s^{-1}; Fig. 3b), there are two precipitation maxima in the SM11 simulation. The first of these is located at about 390 km which is also the location of the precipitation maximum for the SO11 case. The second maximum for the SM11 case is loccated at 600 km. This location coincides with the location of the precipitation maxima for the MO11 case. The reader may note that the maximum for the SM11 case located at 390 km is larger than that for the SO11 simulation, while the maximum located at 600 km is smaller than that for the MO11 simulation. The explanation for this is fairly straightforward. As in the supercritical cases, the convection induced by the cold pool, acted to cool the lowest layer of air just upstream of the mountain via evaporation. This cooling increased the stability of the flow impinging on the mountain shifting the flow to a lower Froude number flow regime. A return flow developed shortly after 3 h in the SM11 case. The resulting flow pattern upstream of the mountain was one of positive y vorticity that acted to enhance postive vertical velocity along the leading edge of the upstream propagating density c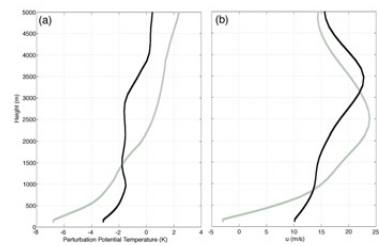urrent associated with the cold air perturbation (consistent with the theory presented in Weisman and Rotunno 2004) and reduce vertical motions along the peak and upslope of the mountain.

The accumulated preciptation for the subcritical cases ($U = 7$ m s^{-1}) is shown in Fig. 3c. According to this figure, the SM7 case is characterized by a precipitation maximum that is greater than that in either the SO7 or MO7 cases. Furthermore, the maximum in the SM7 case is positioned farther upstream than in the other cases. An additional perspective of the preciptation evolution can be gained through inspection of Fig. 5. This figure shows a Hovmöller diagram of rainrate for the SM7 case. Precipitation was initially triggered at 400 km due to the initial cold pool. There two density currents associated with this convection, one that propagates upstream and one that propagates downstream, toward the mountain. Fifty minutes into the simulation, precipitation was also triggered through orographic lifting at about 600 km. This precipitation system propagated upstream. Notice that when the system associated with the pre-existing convection merged with the orographically induced system (at about 3 h), the precipitation rates increased. This merged system produced two density currents, one that propagated downstream and over the orography and another that propagated rapidly upstream and eventually

Figure 4: (a) Perturbation potential temperature at $x = 500$ km for the SM15 (green) and the MO15 (red) cases. (b) The u wind speeds at 500 km for the SM15 (green) and MO15 (red) cases.

phased with the upstream propagating density current associated with the original cold pool. The merging

of these two density currents, which appears to have occurred at about 8 h, led to increased precipitation rates. At about this same time, the merged density currents began to propagate upstream more rapidly than the density current associated with the cold pool had been moving.

4. CONCLUSIONS

This research examines how pre-existing convection behaves as it impinges on orography for different Froude number flow regimes. For low F_w flow, the heaviest precipitation was positioned well upstream of the orography. Furthermore, it was noted that the total accumulated precipitation in this flow regime was much larger than in either the MO or SO cases. For critical flow, the SM cases had two maxima in precipitation. Each of the maxima was colocated with the maxima in the SO and MO cases. For supercritical flow, the precipitation maximum in the SM case was positioned over the mountain peak. This maximum was greater than that in the corresponding MO simulation. Differences in accumulated precipitation between the critical and supercritical cases for the SM and MO simulations can be attributed to the stabilization of the lowest layers upstream of the mountain by evaporative cooling. This stabilization shifts the flow impinging on the orography to a lower Froude number flow regime and reduces the vertical motion over the peak of the mountain.

Preliminary analyses suggest there is a secondary regime within the subcritical flow regime wherein the downstream propagating precipitation system associated with the cold pool is completely blocked by the orography. Further study of this phenomenon is ongoing.

Figure 5: Hovmöller diagram of rainrate (mm hr^{-1}) for the SM7 case.

REFERENCES

Bougeault, P., P. Binder, A. Buzzi, R. Dirke, R. Houze, J. Kuettner, R. B. Smith, R. Steinacker, and H. Volkert, 2001: The MAP special observing period. *Bull. Amer. Meteor. Soc.,* **82**, 433-462.

Chen, S.-H. and Y.-L. Lin, 2004: Effects of the basic wind speed and CAPE on flow regimes associated with a conditionally unstable flow over a mesoscale mountain. *Meteor. Atmos. Phy.*, in press.

Chu, C.-M., and Y.-L. Lin, 2000: Effects of orography on the generation and propagation of mesoscale convective systems in a two-dimensional conditionally unstable flow. *J. Atmos. Sci.,* **57**, 3817-3837.

Lin, Y.-L., R. D. Farley, and H. D. Orville, 1983: Bulk parameterization of the snow field in a cloud model. *J. Climate and Appl. Meteor.,* **22**, 40-63.

Teng, J.-H, C.-S. Chen, T.-C. C. Wang, and Y.-L. Chen, 2000: Orographic effects on a squall line system over Taiwan. *Mon. Wea. Rev.*, **128**, 1123-1138.

Weisman, M. L., and R. Rotunno, 2004: A theory for strong long-lived squall lines revisited. *J. Atmos. Sci.*, **61** 361-382.

Xue, M. , K. K. Droegemeier, V. Wong, A. Shapiro, K. Brewster, F. Carr, D. Weber, Y. Liu, and D.-H. Wang, 2001: The advanced regional prediction system (ARPS) - A multiscale nonhydrostatic atmospheric simulation and prediction tool. Part II: Model physics and 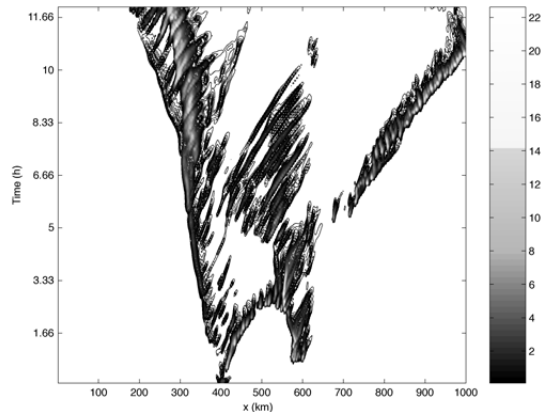applications. *Meteor. Atmos. Phys.*, **76**, 134-165.